Journal of Materials Chemistry A

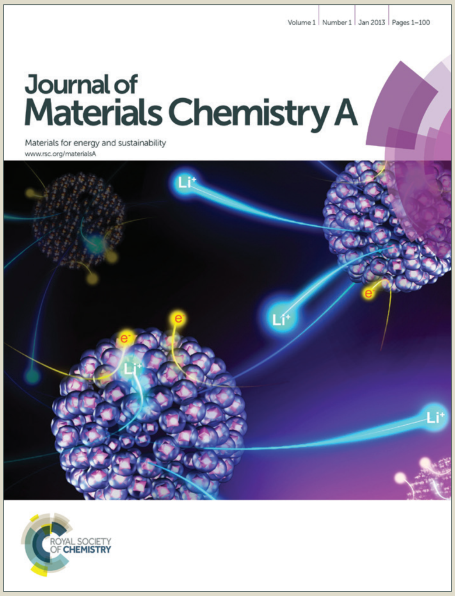

ROYAL SOCIETY OF CHEMISTRY

www.rsc.org/materialsA

Journal of Materials Chemistry A

RSC Publishing

ARTICLE

Cite this: DOI: 10.1039/x0xx00000x

A new Pb(IV)-based photocathode material Sr_2PbO_4 with good light harvesting ability

Dan Zhao[‡], Jing-Feng Han[‡], Jun-Yan Cui, Xu Zong and Can Li*

Received 00th January 2015,
Accepted 00th January 2015

DOI: 10.1039/x0xx00000x

www.rsc.org/

Crystalline plumbate Sr_2PbO_4 has been synthesized by high temperature flux method and characterized by X-Ray powder diffraction analysis, UV-Vis spectrum, theoretical studies and SEM analysis. The results show that Sr_2PbO_4 has indirect optical transitions with energy about 1.75 eV which can be assigned to the electron transfer from state of O-2*p* to mixed states of O-2*p* and Pb-6*s*. The photoelectrochemical properties of Sr_2PbO_4 were studied for the first time, indicating that this material has p-type conductivity. The measured current density at intensity of 47 $\mu A \cdot cm^{-2}$ makes Sr_2PbO_4 to be a promising photocathode material for visible-light-driven water splitting.

1 Introduction

Over the course of past forty years, photocatalytic and photoelectrochemical (PEC) water splitting using a heterogeneous photocatalyst has attracted considerable attention as a potential means of converting solar energy into chemical energy in the form of H_2.[1-5] The research was initially triggered by the potential of TiO_2-based PEC reactions for the decomposition of water into H_2 and O_2 in the beginning of the 1970s.[6] In this field, one of the most important issues is the development of suitable semiconductors as photocatalysts. The number of semiconductor candidates for solar water splitting is limited, and careful materials design is required to obtain an efficient photocatalyst. It seems that the important factors for the efficiency of photocatalysts are as follows: (i) possess the ability to harvest visible light to utilize the main part of the solar spectrum; (ii) have suitable band alignment with water redox potentials; (iii) remain stable in water under irradiation; (iv) have high surface areas and high crystallinity.

Until now, a wide range of semiconducting materials have been developed as photocatalysts for water splitting. Most of these materials are oxide-based compounds containing metal ions of Ti^{4+}, Zr^{4+}, Nb^{5+}, Ta^{5+}, or W^{6+} with d^0 electronic configuration and Cu^+, Ga^{3+}, In^{3+}, Ge^{4+}, Sn^{4+}, or Sb^{5+} with d^{10} electronic configuration. For example, it is reported that d^{10} electronic configuration cuprous oxide (Cu_2O) with band gap of 1.9~2.2 eV is a viable candidate to produce hydrogen by direct water photolysis using visible light with little or no external bias.[7-9] The tops of the valence of these materials bands usually consist of O-2*p* orbitals, which are located at *ca.* +2.94 V or higher *vs.* SHE, while the O_2/H_2O redox potential is at +1.23 V *vs.* SHE. If the bottom of the conduction band of a oxide is more negative than the water reduction potential, the band gap inevitably is larger than 3.0 eV, corresponding to the ultraviolet (UV) light region which shares only around 4% of the solar radiation spectrum to render the material inactive in the visible-light region.

In order to overcome this limitation, many methods have been developed to extend their light absorption into the visible region, such as converting the oxides into (oxy)nitrides. The valence band of (oxy)nitrides is formed by N-2*p* orbitals or hybridized orbitals of O-2*p* and N-2*p*, then the top of the valence band is negatively shifted, resulting in a smaller band gap for the (oxy)nitrides than for the corresponding metal oxides. For example, the visible-light-responsive materials $Sr_5Ta_4O_{15-x}N_x$,[10] $BaTaO_2N$,[11-14] $SrNbO_2N$,[15] $LaTaON_2$,[16, 17] TaON,[18-21] and $(Ga_{1-x}Zn_x)(N_{1-x}O_x)$,[22-24] have been extensively investigated for solar water splitting. Similarly, valence bands of metal (oxy)sulfide photocatalysts are usually composed of S-3*p* orbitals, which resulting in the formation of narrow band gaps. These materials can utilize up to 500 – 600 nm visible light. For example, (oxy)sulfide $Sm_2Ti_2S_2O_5$ is a kind of visible light-driven photocatalysts with a band gap of 2.0 eV and shows stable photocatalytic H_2 or O_2 evolution in the presence of sacrificial reagents.[25-31] However, (oxy)nitrides as well as (oxy)sulfides are not stable enough upon light illumination, and photocorrosion or photodissolution may occur on a photocatalyst surface during photocatalytic reaction. Doping foreign elements into a semiconductor with a wide band gap to extend the optical absorption edge is another effective strategy for developing photocatalysts available for visible-light-driven water splitting, including Cr^{3+},[32-34] Ni^{2+},[35-38] and Co^{2+},[39-41] doping, etc. Unfortunately, doping metal cations may create defect sites or introduce level traps acting as charge recombination centers. Therefore, the most reliable candidates for visible-light-driven photocatalysts would be single phase metal oxides with the narrow band gap to harvest visible light.

Since semiconductors with suitable redox potentials are rare and redox power is weakened by band gap narrowing, developing new materials effective for water splitting under visible-light irradiation remains one of the most challenging tasks for solar-energy utilization. It has been reported that Pb(II)-based oxides absorbed visible light and exhibited good photocatalytic activities for water decomposition under visible light irradiation, such as $PbTiO_3$,[42,43] $PbBi_4Ti_4O_{15}$, $K_{0.5}La_{0.25}Bi_{0.25}Ca_{0.75}Pb_{0.75}Nb_3O_{10}$,[44] and $PbBi_2Nb_2O_9$ [45,46]. This was attributed to the additional hybridization of the occupied Pb-6*s* and O-2*p* orbitals in these compounds, which pushes up the position of the valence band. As well as Pb(II)-based oxides oxides, Pb(IV)-based oxides are also interesting materials as the candidates of visible-light sensitive oxides. The red or black appearance of Pb(IV)-based oxides shows their good light-harvesting ability. However, as far as we know, the photocatalytic activity as well as PEC activity of Pb(IV)-based oxides has not been reported so far.

On the other hand, the defects and boundaries in the semiconductor are believed to act as recombination centers vanishing the excited electron and hole pairs. And the purity and the degree of crystallinity of the semiconductor crystallites would be one of the determining factors for the photocatalytic as well as PEC efficiency. In other words, fine single crystals with fewer defects would be ideal for the semiconductor photocatalysts. Flux method is one of the simplest, highly cost-effective approaches accessible to obtain large single crystals with fewer defects compared to conventional solid state reaction. Herein, we applied the flux method to prepare crystalline plumbate Sr_2PbO_4, whose crystal structure features orthorhombic space group *Pbam*.[47,48] Then we use electrophoretic deposition method to prepare the electrode and measure the photocurrent of Sr_2PbO_4 under visible light irradiation. Moreover, we carry out the calculation of crystal energy band structure and density of states (DOS) with the density functional theory (DFT) method in order to understand the chemical bonding property and electronic origin of optical transition of Sr_2PbO_4.

2 Experimental section

2.1 Synthesis

Raw materials of KCl, K_2CO_3, $SrCl_2 \cdot 6H_2O$ and PbO were purchased from the Shanghai Reagent Factory. All of them were analytically pure from commercial sources and used without further purification. Single crystals of Sr_2PbO_4 were grown by using KCl—K_2CO_3—$SrCl_2$ as flux in a corundum crucible with lid from reagent-grade mixtures of KCl (3.599g), K_2CO_3 (3.333g), $SrCl_2 \cdot 6H_2O$ (9.659g) and $Pb(NO_3)_2$ (4.000g) at the molar ratio of 4:2:3:1. The mixture of the raw material was ground and heated in the crucible at 400 ºC for 5 h. After additionally ground, the mixture was heated in an electric furnace to 850 ºC, held for 3 h, and then cooled slowly to the temperature of 650 ºC at the rate of 10 ºC/h and to room temperature by turning off the power. After washing in water, prism-shaped red single crystals of Sr_2PbO_4 were purified.

2.2 Characterizations

XRD measurement was carried out on a Rigaku D/Max-2500/PC powder diffractometer (Cu K*α* radiation) with an operating voltage of 40 kV and an operating current of 200 mA. The scan rate of 5º /min was applied in the range of 5~75º at a step size of 0.02º. Optical diffuse reflectance spectra were measured at room temperature with a UV-Vis spectrophotometer (JASCO V-550) equipped with an integrating sphere. The samples were ground into fine powder and pressed onto a thin glass slide holder. $BaSO_4$ plate was used as a standard (100% reflectance). The absorption spectra were calculated from reflectance spectra using the Kubelka－Munk function: $F(R) = (1-R)^2/2R$.[49] The minima in the second-derivative curves of the Kubelka－Munk function are taken as the position of the absorption bands. The morphology and energy dispersive spectrometer (EDS) were examined by scanning electron microscopy (SEM; Quanta 200 FEG, FEI and S-5500, Hitachi).

2.3 Electrode Preparation and Photoelectrochemical Measurements

The photoelectrode of Sr_2PbO_4 was prepared by the electrophoretic deposition (EPD) method on F-doped SnO_2 (FTO) glass in a constant voltage mode. As a typical procedure, crystalline sample was ground carefully in an agate mortar in the presence of ethanol for 30 min and then dispersed in acetone (50 mL) with iodine (10 mg). Additional iodine was used to give H^+ by the reaction with acetone and thus made particles positively charged. After that, two FTO glasses were immersed in the solution in parallel at a distance of about 2.5 cm and 40 V of voltage was applied between the electrodes for 5 min using a DC power supply. The coated area used for photocurrent measurement was about 5 × 5 mm. Finally, the electrode was heat treated in air at 450 ºC for 30 min.

The flat-band potential of Sr_2PbO_4 was determined by extrapolation of the Mott–Schottky plots measured on a standard three-electrode cell electrochemical workstation (CHI660A, Shanghai Chenhua Instruments, China). In this system, a Pt plate was used as counter electrode, a saturated calomel electrode (SCE) was employed as reference electrode, and the electrolyte was 0.5 M Na_2SO_4 (pH = 7.0, adjusted by NaOH and H_2SO_4) solution. A scanning potentiostat was used to measure photocurrents under chopped irradiation from a 300 W Xe lamp (Perfectlight PLX SXE300C) equipped with an optical cutoff filter (Kenko, L-42; $\lambda > 420$ nm). The light intensity and spectrum during the PEC measurements was shown in Fig. S2. The photocurrent was measured by linear sweep voltammetry from -0.5 to 0.1 V (*vs.* SCE) with a scan rate of 0.01 V/s. The light irradiation came from the back side of FTO glass.

2.4 Computational descriptions

The crystallographic data of distrontium plumbate Sr_2PbO_4 from Troemel' report was used to calculate its energy band structures with no further geometry optimizations. The calculations use the total-energy code CASTEP,[50-54] which employs pseudopotentials to describe electron-ion interactions and represents electronic wave functions using a plane-wave basis set. The total energy and properties were calculated within the framework of the Perdew-Burke-Ernzerhof generalized gradient approximation (GGA-PBE).[55] In addition, the norm-conserving pseudopotentials [56] were employed for Sr, Pb and O, respectively. The total energy and the force convergence thresholds were 1.0×10^{-6} eV/atom and 0.05 eV/Å, respectively. The *k*-point set meshes to define the number of integration points that will be used to integrate the wave function in reciprocal space were 4×2×7 for calculating bond structure, density of states and optical property. The rest parameters used in the calculations were set by the default values of the CASTEP code. Pseudoatom calculations were performed for Sr-$4s^24p^65s^2$, Pb-$5s^25p^65d^{10}6s^26p^2$, and O-$2s^22p^4$.

3 Results and discussion

3.1 Syntheses

We choose flux method to grow crystalline Sr_2PbO_4 used for PEC studies, and the KCl—K_2CO_3—$SrCl_2$ mixed salt which are easily removed by washing with water after the reaction was chosen as flux. The excess $SrCl_2$ was used because the Sr cation is common to Sr_2PbO_4, and this may prevent the generation of $SrPbO_3$ phase in the products. Moreover, it has a relatively low melting point (874 ºC). Compound $Pb(NO_3)_2$, which is thought to be easy for the generation of Pb(IV) cations in the molten condition, was used as the source of lead. The synthesis of Sr_2PbO_4 can be expressed by the following equation in molten salt at 850ºC.

$$2SrCl_2 + Pb(NO_3)_2 \rightarrow Sr_2PbO_4 + 2NO_2$$

The final product Sr_2PbO_4 was washed up in water for several times to remove flux salts. Such a treatment could prove the fact that Sr_2PbO_4 is stable enough in water condition, which is one of the most basic requirements for a photocatalyst.

As a trial, we used KCl—$SrCl_2$ mixture as the flux to grow single crystals of Sr_2PbO_4. However, a large amount of impurity phase with amorphous black powder appearance was produced, whose chemical composition was not studied at present stage. Hence, we tentatively put forward that K_2CO_3 in the molten flux play an important role to stable the product Sr_2PbO_4, as well as other plumbates. According to this kind of thought, we tried to synthesis other plumbates, that is Ca_2PbO_4 [57,58] and Ba_2PbO_4 [59], with the similar method. Red needle-like crystals and black block-shaped crystals, respectively for Ca_2PbO_4 and Ba_2PbO_4, was obtained after turning off the electric furnace. Sample Ca_2PbO_4 can be purified by washing up in water, which could be confirmed by an X-Ray powder diffraction study (Fig. S1). However, it seems that Ba_2PbO_4 is not stable enough in water condition like Ca_2PbO_4 and Sr_2PbO_4. Thus we conclude that pure phase of Ba_2PbO_4 is difficult to be obtained as a purified phase using this method. Further studying for Ca_2PbO_4 and Ba_2PbO_4 is in progress.

3.2 Characterizations

After ground large single-crystals into powder, the crystal structure of Sr_2PbO_4 was analyzed by Powder-XRD measurement. As shown in Fig. 1a, all of the diffraction peaks coincide with the powder pattern simulated from single-crystal date (orthorhombic space group *Pbam*, a = 6.159(1) Å, b = 10.078(2) Å, c = 3.502(1) Å) [47], as well as the standard card of No. 22-1434 [48]. The structure of Sr_2PbO_4 contains chains of edge-shared $[PbO_6]$ octahedra running along the *c*-axis. These chains are separated and charge-balanced by Sr^{2+} chains surrounding the octahedral chains, as shown in Fig. 1a. The $[PbO_6]$ features a compressed octahedral geometry with axial Pb—O bond lengths of 2.100(95) Å and equatorial Pb—O bond lengths of 2.270(77) Å.

Furthermore, one of the most striking feature of experimental XRD pattern is the relative intensities of the (110) diffraction peak are stronger than (111) peak, which presents a striking contrast to the simulated pattern. The results indicate that (110) facet are more exposed than (111) facet. This can also be seen in the SEM images. As shown in Fig. 2a and 2b, our product of Sr_2PbO_4 show smooth surface, regular prism shape and excellent crystallinity. At high magnification (Fig. 2c), large compact particles with perfect cuboid shape were observed for Sr_2PbO_4 sample, which is coincide with the orthorhombic unit cell of Sr_2PbO_4. There was a negligible quantity of small irregular particles adhering to the decagonal particles. The formation of domains with smooth surfaces was observed. These domains ended with well-defined walls, the edges of which were relatively very sharp. On the other hand, the atomic ratio of Sr : Pb determined by energy-dispersive spectrometry (EDS) was 31.05 : 16.50 (Fig. 2d). Since samples are unpolished and X-ray corrections may be approximate especially for light elements, the results were in agreement with that determined from the formula Sr_2PbO_4.

As shown in Fig. 3, the UV−Vis diffuse reflectance spectrum of Sr_2PbO_4 was measured ranging from 200 to 850 nm after ground single crystals into powder. The absorption edge is around 710 nm (1.75 eV), which might be considered as the band gap of Sr_2PbO_4. This suggests that the present material can harvest visible light in the wavelength range of 420–710 nm and has a possibility of utilizing visible light for PEC.

3.3 Band structure, density of states and chemical bonds

The calculated band structure of Sr_2PbO_4 along high-symmetry points of the first Brillouin zone are plotted in Fig. 4. It is observed that the top of the valence bands (VBs) is a little dispersion and close to the Fermi level (0.0 eV), and the bottom of the conduction bands (CBs) exhibits obvious dispersion too. The state energies of the lowest conduction band (L-CB) and the highest valence band (H-VB) at some points are listed in Tab. 1. The lowest energy of CBs is localized at G point and the highest energy (0.00 eV) of VBs is localized at Z point. However, the energy at G-point of H-VB (-0.140 eV) is close to the energy at Z-point of H-VB, therefore, it is almost to say that Sr_2PbO_4 is a semiconductor with indirect or approximately direct band-gap.

Comparing with the experimental band gap of 1.75 eV, the calculated indirect band gap of 1.25 eV is small. The discrepancy is due to the limitation of DFT method that generally underestimates the band gap in semiconductors and insulators.[60-62] As a result, scissor operator of 0.5 eV, was applied for the calculation of DOS as well as optical property of Sr_2PbO_4.

In order to better understand the nature of the electronic band structures, the density of total states (TDOS) of Sr_2PbO_4 and projected density of states (PDOS) for Sr, Pb, and O elements ranging from -40 to 20 eV calculated by PBE are presented in Figure 5. The regions below the Fermi level contain 49 bands (2 units per unit cell) and can be divided into five regions. The bottom-most VB region with energy located at around -31.5 eV is composed of Sr-4*s* states. The bands ranging from -17.8 eV to -12.0 eV arises mainly from mixed states of Sr-4*p*, Pb-5*d* and O-2*s*. The bands at around -6.5 eV are composed of Pb-6*s* mixed with O-2*s*2*p* states. The fourth region ranging from -3.5 eV to -2.0 eV arises mainly from Pb-6*p* states. The highest VB region just below the Fermi level is dominated by the O-2*p* states, mixing with small amount of Sr-5*s* states.

The most obvious feature of the band structure of Sr_2PbO_4 is that the CBs just above the Fermi level are composed of mixed states of Pb-6*s* and O-2*p* states. The hybridization between Pb-6*s* and O-2*p* states would push down the position of the conduction band giving the smaller band gap. Therefore, we believe that the optical absorptions at low energy region (about 710 nm) can be mainly ascribed to the charge transitions from O-2*p* states to mixed states of Pb-6*s* and O-2*p*. Unlike Sr_2PbO_4, the highest VBs of Pb(II)-based compounds (such as $PbTiO_3$ [63]) are mainly composed of Pb-6*s* and O-2*p* hybridizated states, and the lowest CBs contain no ingredient of Pb-6*s* orbits, which could only absorb visible light up to about 450 nm. Since Pb(IV)-based oxide Sr_2PbO_4 can absorb a larger amount of visible light than Pb(II)-based oxides, we think Sr_2PbO_4 is a more promising photocatalyst than Pb(II)-based oxides.

In addition, we used the population analyses to elucidate the nature of the electronic band structure and chemical bonds. The calculated Mulliken bond orders of the Sr—O and Pb—O bonds are 0.05–0.26 and 0.26–0.52 e (covalent single-bond order is generally 1.0 e), respectively. Accordingly, we can say that the covalent character of the Pb—O bond is larger than that of the Sr—O bond, and the ionic character of the Sr—O bond is larger than that of the Pb—O bond. We believe that the covalent character of Pb—O bond is beneficial for the charge transfer from O-2*p* states to Pb-6*s* states and is therefore beneficial for the separation of photogenerated electrons and holes.

3.4 PEC Properties

Since the quality of an electrode is an important factor for high photoelectrochemical performance, we examined the morphological characteristics of our electrode prepared by electrophoretic deposition (EPD) method by scanning electron microscopy. As shown in Fig. 6, the electrode prepared by electrophoretic deposition (EPD) is tightly stacked by Sr_2PbO_4 particles within a broad range from nanoscale to microscale. Considering the fact that large quantity of grain boundaries and loose inter-particle connection may be possibly detrimental for the continuous electron transport between Sr_2PbO_4 particles, we think it definitely still have some room for improvement.

In order to find the band edge positions of the Sr_2PbO_4, Mott–Schottky (M–S) plot of the prepared electrode was measured at pH=7 (consistent with the test condition of photoelectrochemical reaction). The flat-band potential Sr_2PbO_4 was obtained by the extrapolation of the M–S (C^{-2} *vs.* E, electrode potential) using the following equation: $C_{sc}^{-2} = 2(E - E_{fb} \cdot - \kappa T/e)/e\varepsilon\varepsilon_0 N_D$.[64] As shown in Fig. 7, it can be seen that the E_{fb} of Sr_2PbO_4 is about 1.21 V (*vs.* RHE). In addition, the slope in the linear region of the plot is negative, which serves as an indication that the synthesized Sr_2PbO_4 is a p-type semiconductor. It is generally known that the VB potentials (EVB) of p-type semiconductor is very close to (about 0.10 V more positive) the flat-band potentials, so it can be roughly deduced that the valance band (VB) position of Sr_2PbO_4 is about 1.31 V (*vs.* RHE). By further considering that the band gap of Sr_2PbO_4 is 1.75 eV and, the conduction band of Sr_2PbO_4 can be estimated to be roughly ca. -0.44 eV (*vs.* RHE). Hence, the band edge positions of the p-type Sr_2PbO_4 is estimated and shown in the inset of Fig. 7, indicating that Sr_2PbO_4 has enough driving force for proton reduction and water oxidation.

The photoelectrochemical behaviour of Sr_2PbO_4 electrode was evaluated by a linear sweep voltammetric technique in 0.5 M Na_2SO_4 solution (pH=7) under chopped light illumination of 300 W Xe lamp with a 420 nm filter. No sacrificial reagents such as the electron acceptor or electron donors were added into solution to generate a photocurrent. As expected for p-type semiconductor, the electrode of Sr_2PbO_4 generates cathodic photocurrent under visible light illumination. As shown in Fig. 8, the on-set potential of the $SrPb_2O_4$ photocathode is estimated to be -0.05 V vs. SCE. Upon repetitive irradiation with xenon light on and off, a clear photocurrent response was observed. The cathode photocurrent was reached quickly without delay and was stable without a decrease in the intensity, providing an effective and repeatable photocurrent response. The current density of 47 $\mu A \cdot cm^{-2}$ at 0.4 V vs. SCE indicates that Sr_2PbO_4 holds a promise for photoelectrochemical water splitting under visible light illumination.

4 Conclusions

In summary, high-temperature flux synthesis afforded a crystalline plumbate Sr_2PbO_4 in mm scale, which was then characterized by X-Ray diffraction analysis, UV-Vis spectrum, theoretical studies, SEM analysis and photoelectrochemical measurements. The results show that Sr_2PbO_4 has indirect optical transitions with energy about 1.75 eV which can be assigned to the charge transfer from O-2p to O-2p and Pb-6s states. Such a narrow band makes it can harvest visible light up to 710 nm. The photoelectrochemical properties of Sr_2PbO_4 were studied for the first time, indicating that this material has p-type conductivity. This work not only develops a new photoelectrode material Sr_2PbO_4 but also supplies a strategy for preparing other crystalline Pb(IV)-based oxides for photoelectrochemical water splitting, as well as photocatalytic water splitting.

Notes

The authors declare no competing financial interest.
Address: State Key Laboratory of Catalysis, Dalian Institute of Chemical Physics, Chinese; Academy of Sciences, Dalian National Laboratory for Clean Energy, Dalian, 116023,
China.
‡: These authors are co-first authors.
*Corresponding author: canli@dicp.ac.cn (Can Li)
Fax: +86-411-84694447; Tel: +86-411-84379760

Acknowledgements

This work was financially supported by 973 National Basic Research Program of the Ministry of Science and Technology (Grant 2014CB239403), National Natural Science Foundation of China (No. 21201056).

References

1 H. Tong, S. Ouyang, Y. Bi, N. Umezawa, M. Oshikiri and J. Ye, *Adv. Mater.*, 2012, **24**, 229.
2 X. Chen, S. Shen, L. Guo and S. S. Mao, *Chem. Rev.*, 2010, **110**, 6503.
3 K. Maeda and K. Domen, *MRS Bull.*, 2011, **36**, 25.
4 Y. Ma, X. Wang, Y. Jia, X. Chen, H. Han and C. Li, *Chem. Rev.*, 2014, **114**, 9987.
5 A. Kudo and Y. Miseki, *Chem. Soc. Rev.*, 2009, **38**, 253.
6 A. Fujishima and K. Honda, *Nature*, 1972, **238**, 37.
7 C.-C. Hu, J.-N. Nian and H. Teng, *Sol. Energy Mater. Sol. Cells*, 2008, **92**, 1071.
8 C. M. McShane and K.-S. Choi, *J. Am. Chem. Soc.*, 2009, **131**, 2561.
9 J.-N. Nian, C.-C. Hu and H. Teng, *Int. J. Hydrogen Energy*, 2008, **33**, 2897.
10 S. Chen, J. Yang, C. Ding, R. Li, S. Jin, D. Wang, H. Han, F. Zhang and C. Li, *J. Mater. Chem.*, 2013, **1**, 5651.
11 M. Higashi, K. Domen and R. Abe, *J. Am. Chem. Soc.*, 2013, **135**, 10238.
12 K. Maeda and K. Domen, *Angew. Chem.*, Int. Ed., 2012, **51**, 9865.
13 A. M. Hafez, N. M. Salem and N. K. Allam, *Phys. Chem. Chem. Phys.*, 2014, **16**, 18418.
14 K. Maeda, D. Lu and K. Domen, *Angew. Chem., Int. Ed.*, 2013, **52**, 6488.
15 K. Maeda, M. Higashi, B. Siritanaratkul, R. Abe and K. Domen, *J. Am. Chem. Soc.*, 2011, **133**, 12334.
16 M. Liu, W. You, Z. Lei, T. Takata, K. Domen and C. Li, *Chin. J. Catal.*, 2006, **27**, 556.
17 L. Zhang, Y. Song, J. Feng, T. Fang, Y. Zhong, Z. Li and Z. Zou, *Int. J. Hydrogen Energy*, 2014, **39**, 7697.
18 G. Hitoki, T. Takata, J. N. Kondo, M. Hara, H. Kobayashi and K. Domen, *Chem. Commun.*, 2002, **16**, 1698.
19 M. Hara, J. Nunoshige, T. Takata, J. N. Kondo and K. Domen, *Chem. Commun.*, 2003, 3000.
20 K. Maeda, M. Higashi, D. L. Lu, R. Abe and K. Domen, *J. Am. Chem. Soc.*, 2010, **132**, 5858.
21 M. Higashi, K. Domen and R. Abe, *J. Am. Chem. Soc.*, 2012, **134**, 6968.
22 K. Maeda, T. Takata, M. Hara, N. Saito, Y. Inoue, H. Kobayashi and K. Domen, *J. Am. Chem. Soc.*, 2005, **127**, 8286.
23 K. Maeda, K. Teramura, D. L. Lu, N. Saito, Y. Inoue and K. Domen, *Angew. Chem., Int. Ed.*, 2006, **118**, 7970.
24 T. Ohno, L. Bai, T. Hisatomi, K. Maeda and K. Domen, *J. Am. Chem. Soc.*, 2012, **134**, 8254.
25 A. Ishikawa, T. Takata, J. N. Kondo, M. Hara, H. Kobayashi and K. Domen, *J. Am. Chem. Soc.*, 2002, **124**, 13547.
26 A. Ishikawa, Y. Yamada, T. Takata, J. N. Kondo, M. Hara, H. Kobayashi and K. Domen, *Chem. Mater.*, 2003, **15**, 4442.
27 K. Maeda and K. Domen, *J. Phys. Chem.* C, 2007, **111**, 7851.
28 M. Yashima, K. Ogisu and K. Domen, *Acta Crystallogr., Sect. B: Struct. Sci.*, 2008, **64**, 291.
29 F. Zhang, K. Maeda, T. Takata and K. Domen, *J. Catal.*, 2011, **280**, 1.
30 F. Zhang, K. Maeda, T. Takata, T. Hisatomi and K. Domen, *Catal. Today*, 2012, **185**, 253.
31 W. Zhao, K. Maeda, F. Zhang, T. Hisatomi and K. Domen, *Phys. Chem. Chem. Phys.*, 2014, **16**, 12051.
32 D. F. Wang,, J. H. Ye, T. Kako and T. Kimura, *J. Phys. Chem. B*, 2006, **110**, 15824.
33 Z. G. Yi, H. Iwai and J. H. Ye, *Appl. Phys. Lett.*, 2010, **96**, 114103.
34 D. F. Wang, Z. G. Zou and J. H. Ye, *Chem. Mater.*, 2005, **17**, 3255.
35 M. Sun, Z. Chen and J. Yu, *Electrochim. Acta*, 2013, **109**, 13.
36 J. Chattopadhyay, R. Srivastava and P. K. Srivastava, *J. Appl. Electrochem.*, 2013, **43**, 279.
37 S. Li, L. Zhang, T. Jiang, L. Chen, Y. Lin, D. Wang and T. Xie, *Chem.-Eur. J.*, 2014, **20**, 311.
38 T. Sun, J. Fan, E. Liu, L. Liu, Y. Wang, H. Dai, Y. Yang, W. Hou, X. Hu and Z. Jiang, *Powder Technol.*, 2012, **228**, 210.
39 H. M. Luo, T. Takata, Y. G. Lee, J. F. Zhao, K. Domen and Y. S. Yan, *Chem. Mater.*, 2004, **16**, 846.
40 M. Z. Selcuk, M. S. Boroglu and I. Boz, *React. Kinet. Catal. Lett.*, 2012, **106**, 313.
41 X. Zhou, J. Shi and C. Li, *J. Phys. Chem. C*, 2011, **115**, 8305.
42 D. Arney, T. Watkins and P. A. Maggard, *J. Am. Ceram. Soc.*, 2011, **94**, 1483.
43 H. G. Kim, O. S. Becker, J. S. Jang, S. M. Ji, P. H. Borse and J. S. Lee, *J. Solid State Chem.*, 2006, **179**, 1214.
44 H. G. Kim, O. S. Becker, J. S. Jang, S. M. Ji, P. H. Borse and J. S. Lee, *J. Solid State Chem.*, 2006, **179**, 1214.
45 H. G. Kim, P. H. Borse, J. S. Jang, E. D. Jeong and J. S. Lee, *Mater. Lett.*, 2008, **62**, 1427.
46 W. Wu, G. Liu, S. Liang, Y. Chen, L. Shen, H. Zheng, R. Yuan, Y. Hou and L. Wu, *J. Catal.*, 2012, **290**, 13.

47 Troemel, M. *Z. Anorg. Allg. Chem.,* 1969, **371**, 237.

48 K. L. Keester and W. B. White, *J. Solid State Chem.*, 1970, **2**, 68.

49 W. W. M. Wendl and H. G. Hecht, Reflectance Spectroscopy, Wiley, New York, 1966.

50. M. Segall, P. Linda, M. Probert, C. Pickard, P. Hasnip, S. Clark and M. Payne, Materials Studio CASTEP version 2, 2002.

51 M. Segall, P. Linda, M. Probert, C. Pickard, P. Hasnip, S. Clark and M. Payne, *J. Phys.: Condens. Mater*, 2002, **14**, 2717.

52 Materials Studio CASTEP version 2.2 Program, developed by Accelrys Inc.

53 V. Milman, B. Winkler, J. A. White, C. J. Pickard, M. C. Payne, E. V. Akhmatskaya and R.H. Nobes, *Int. J. Quantum Chem*, 2000, **77**, 895.

54 J. S. Lin, A. Qteish, M. C. Payne and V. Heine, *Phys. Rev. B*, 1993, **47**, 4174.

55 J. P. Perdew, K. Burke and M. Ernzerhof, *Phys. Rev. Lett*, 1996, **77**, 3865.

56 M. C. Payne, M. P. Teter, D. C. Allan and J. D. Joannopoulos, *Rev. Mod. Phys*, 1992, **64**, 1045.

57 B. Reardon and C. Hubbard, *Z. Anorg. Allg. Chem.*, 1969, **371** 237.

58 A. Teichert and H. Mueller Buschbaum, *Z. Anorg. Allg. Chem.,* 1992, **607**, 128.

59 H. Stoll and R. Hoppe, *Z. Anorg. Allg. Chem.,*1987, **548**, 165.

60 R.W. Godby, M. Schluther and L. J. Sham, *Phys. Rev. B*, 1987, **36**, 6497.

61 C. M. I. Okoye, *J. Phys.: Condens. Matter*, 2003, **15**, 5945.

62 D. Zhao, H. Zhang, Z. Xie, W. L. Zhang, S. L. Yang and W. D. Cheng, *Dalton Trans.*, 2009, 5310.

63 H. G. Kim, O. S. Becker, J. S. Jang, S. M. Ji, P. H. Borse, J. S. Lee, *J. Solid State Chem.*, 2006, **179**, 1214.

64 S. N. Frank and A. J. Bard, *J. Am. Chem. Soc.*, 1975, **97**, 7427.

Table 1. The state energies (eV) of the lowest conduction band (L–CB) and the highest valence band (H–VB) at some *k*-points of Sr_2PbO_4.

k-point	G(0,0,0)	Z(0,0,0.5)	T(-0.5,0,0.5)	Y(-0.5,0,0)	S(-0.5,0.5,0)	X(0,0.5,0)	U(0,0.5,0.5)	R(-0.5,0.5,0.5)
L–CB	1.750	2.747	3.491	2.738	2.748	2.314	3.109	3.535
H–VB	-0.140	0.000	-0.269	-0.234	-0.231	-0.171	-0.117	-0.303

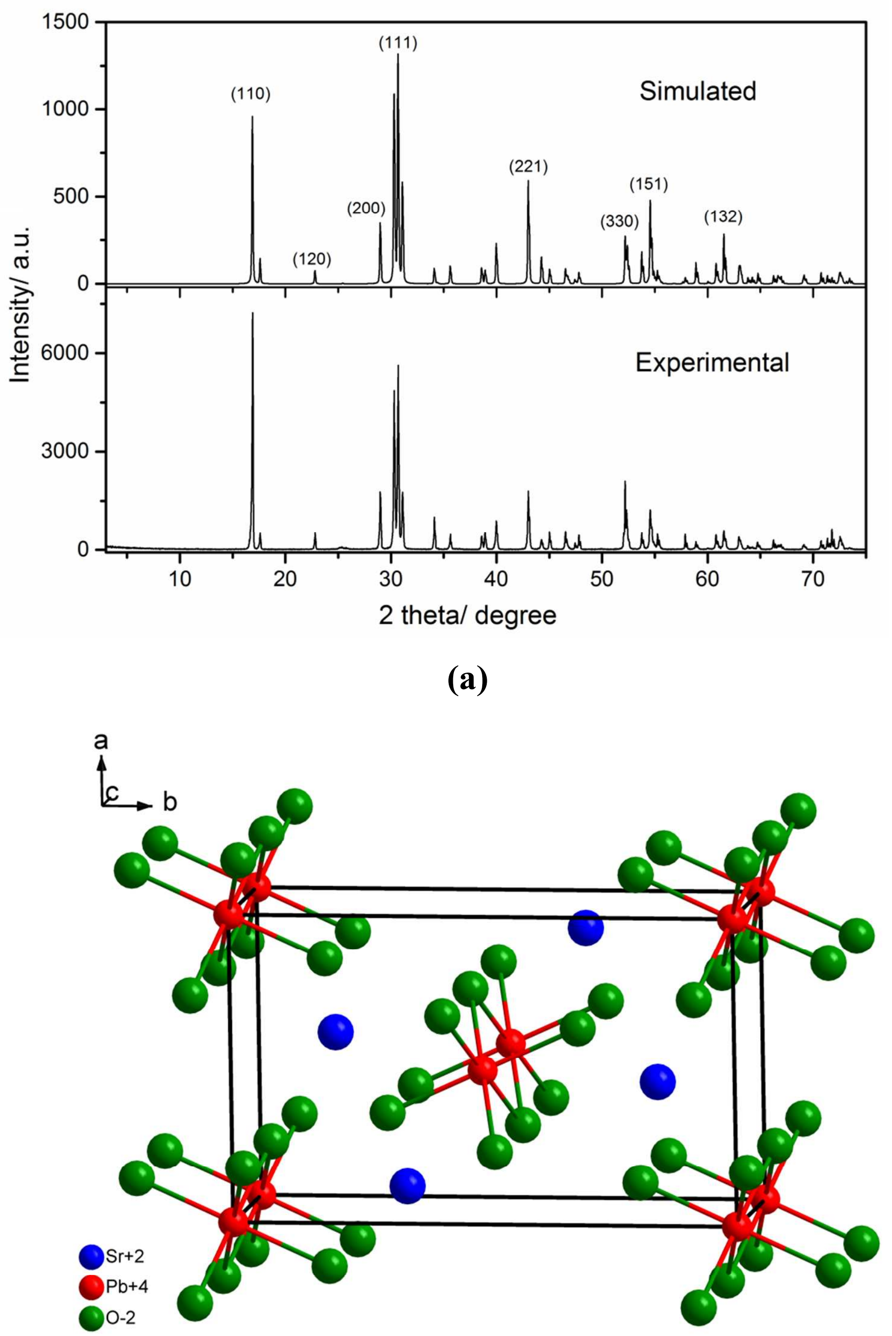

(b)

Figure 1. (a) XRD pattern of Sr_2PbO_4 experimental sample comparing with simulated date from single-crystal; (b) Crystal structure model of Sr_2PbO_4

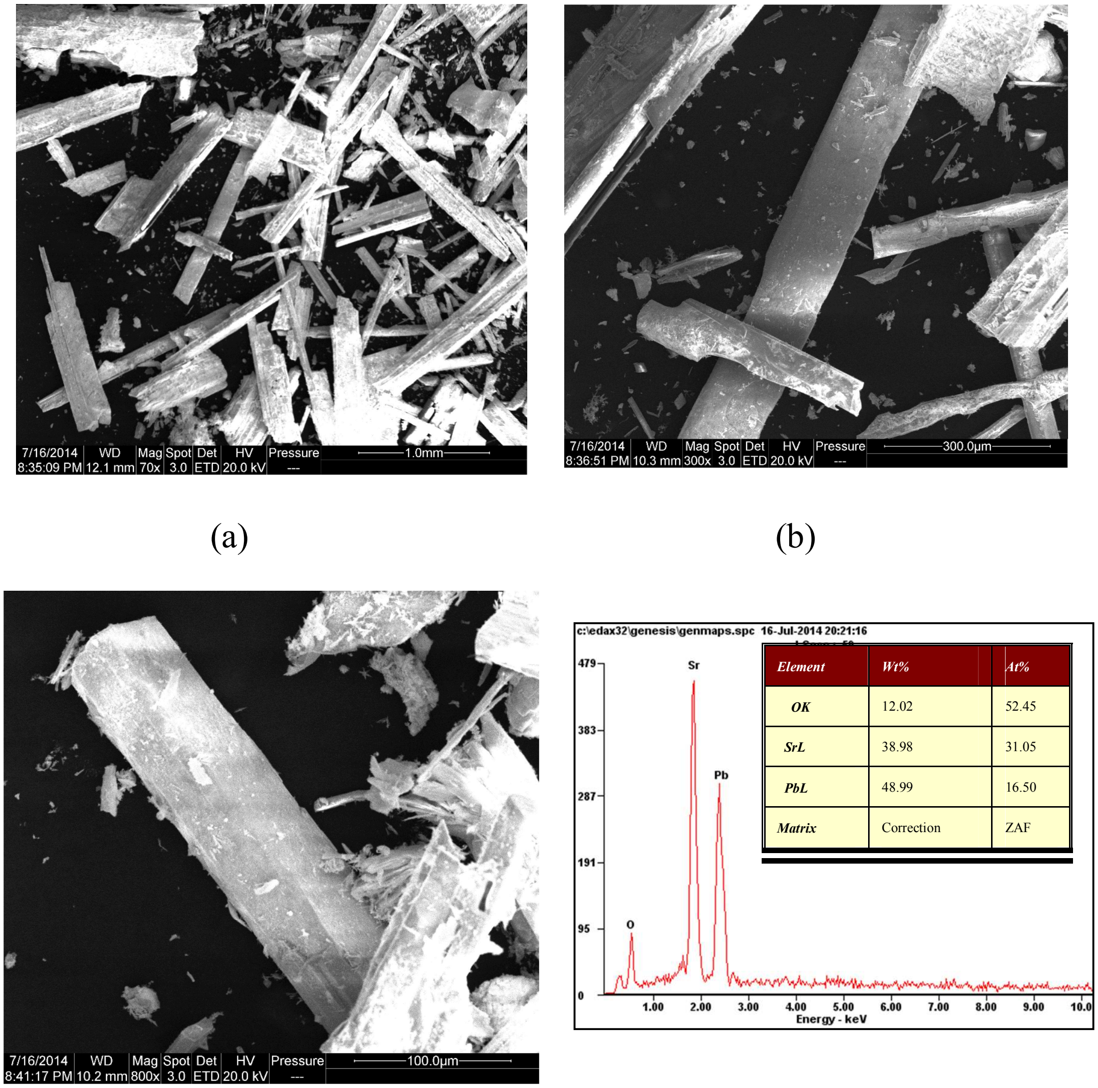

Element	*Wt%*	*At%*
OK	12.02	52.45
SrL	38.98	31.05
PbL	48.99	16.50
Matrix	Correction	ZAF

(a) (b)

(c) (d)

Figure 2. (a)–(c) SEM images of crystalline Sr_2PbO_4; (d) EDS analysis of Sr_2PbO_4

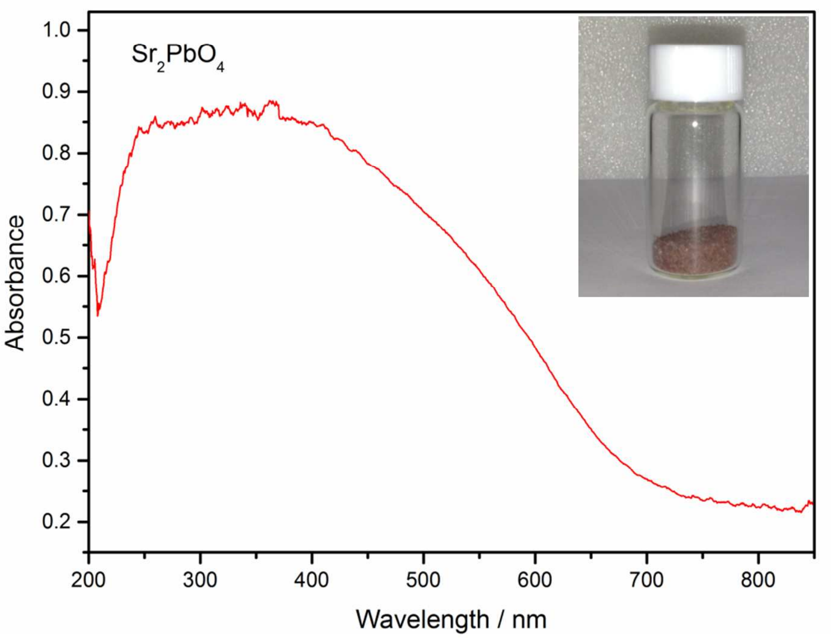

Figure 3. Experimental absorption spectra of Sr_2PbO_4 ranging from 200 to 850 nm

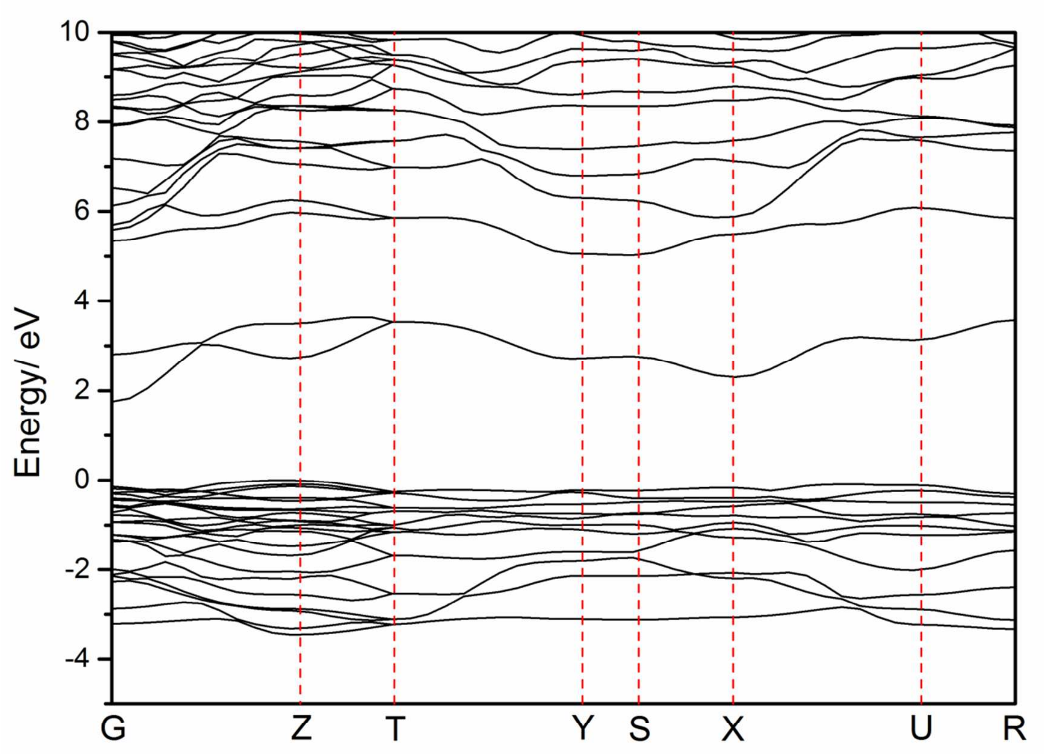

Figure 4. Calculated energy band structure of Sr_2PbO_4 in the range from -5.0 to 10.0 eV (The Fermi level is set at 0.0 eV.)

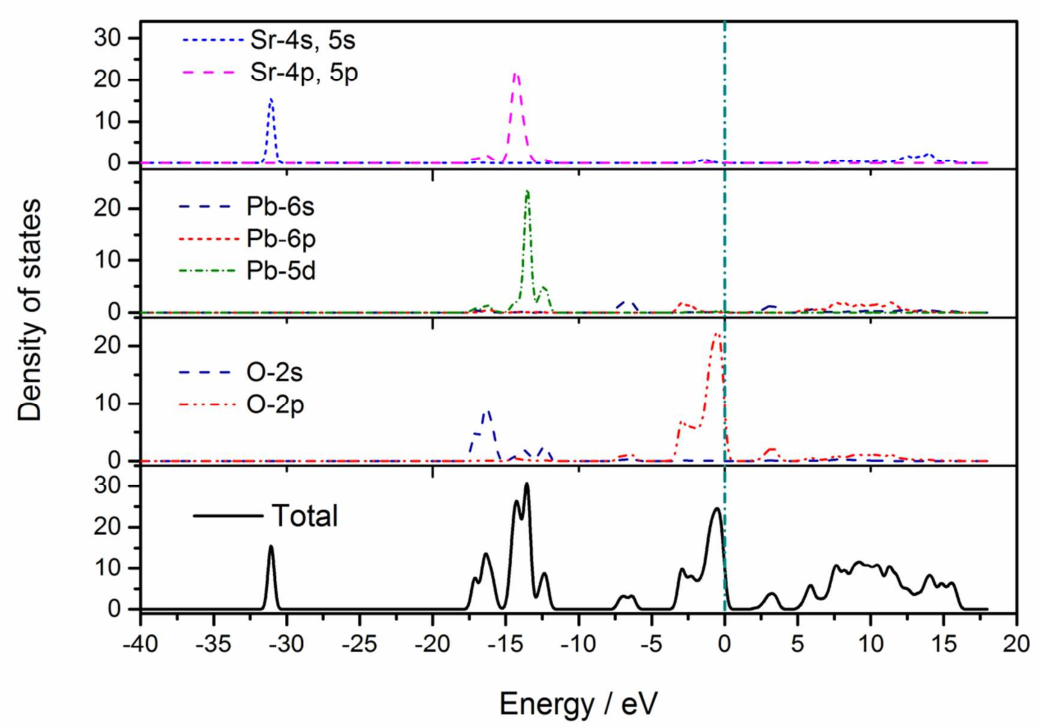

Figure 5. Total and partial DOS of Sr_2PbO_4

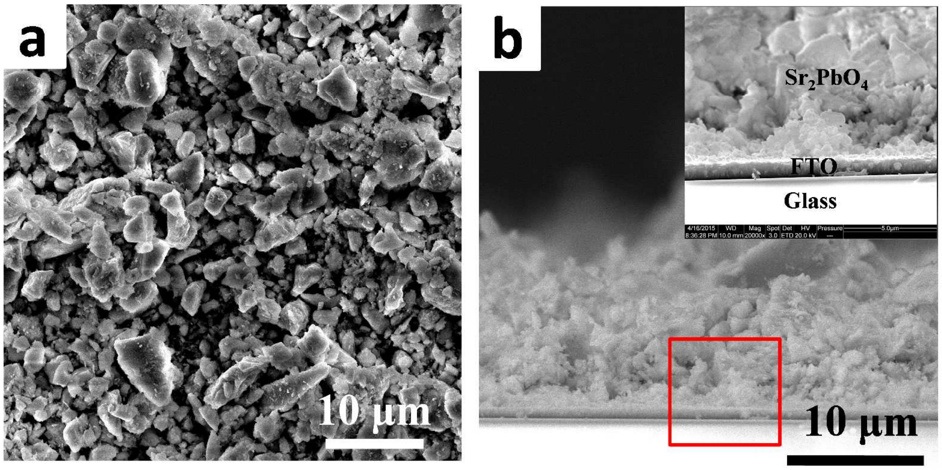

Figure 6. Top (a) and cross sectional (b) SEM images of Sr_2PbO_4 electrode prepared by EPD method.

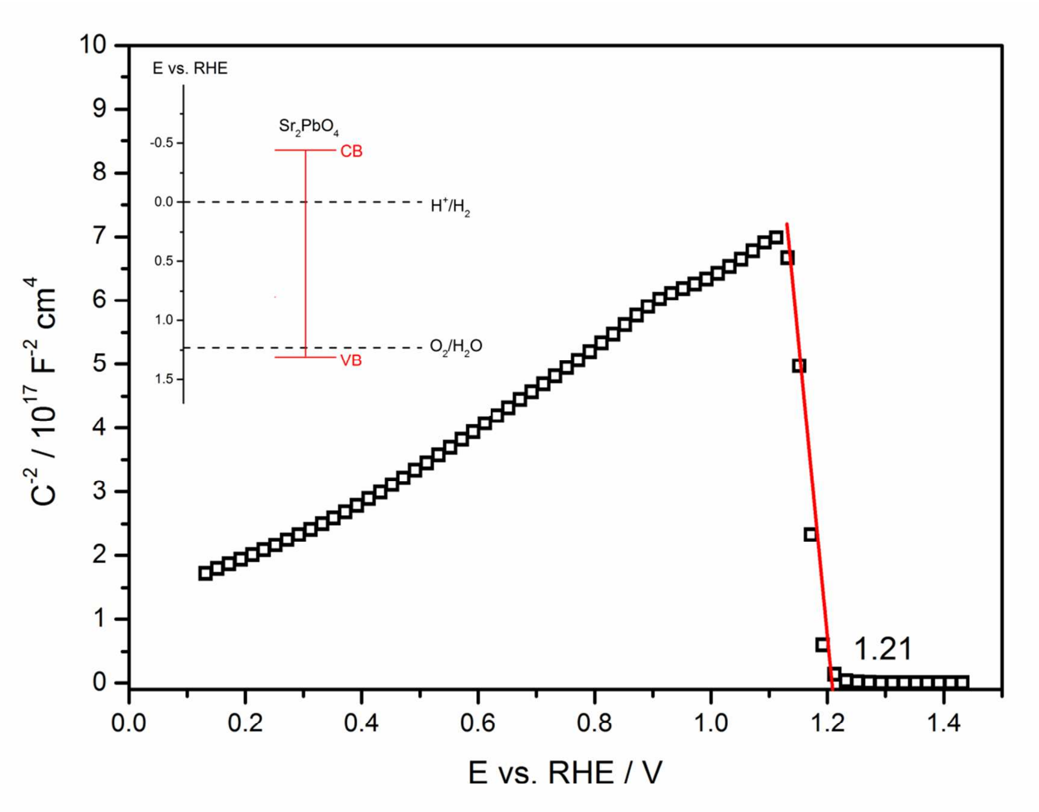

Figure 7. M–S plot of the Sr_2PbO_4 electrode and the estimated band edge positions of Sr_2PbO_4 at pH = 7; (inset). Electrolyte: 0.5 M Na_2SO4 solution (pH = 7, adjusted by NaOH and H_2SO_4), frequency: 3 kHz

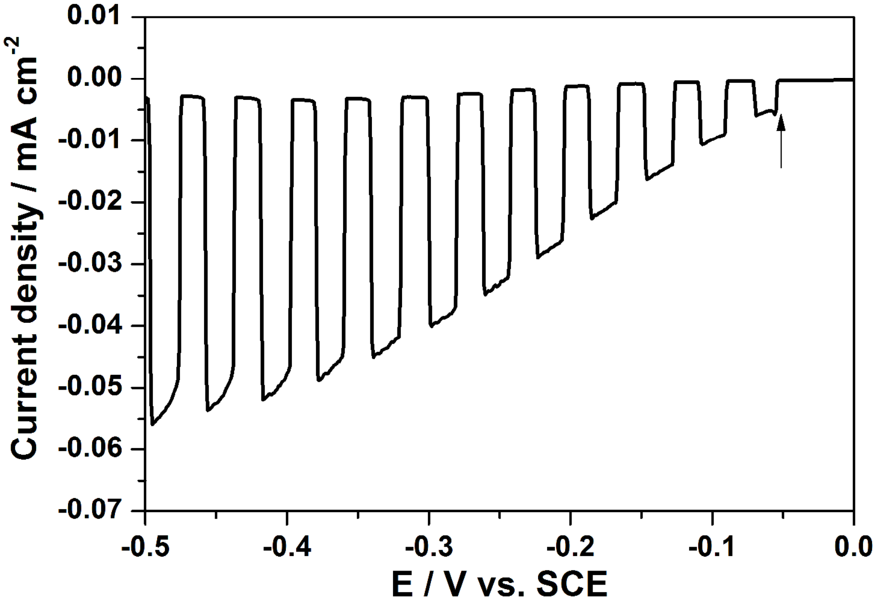

Figure 8. Linear sweep voltammetric scans of Sr_2PbO_4 photocathodes in 0.5 M Na_2SO_4 (pH = 7.0) under chopped light illumination; light source: 300 W Xe lamp (λ≥420 nm, 400 mW cm^{-2}); scanning rate: 20 mV s^{-1}.

This work reported a new p-type photocathode material Sr_2PbO_4 with the visible light harvesting ability up to 710nm.